Supplementary information

Stations localization

Eddies are commonly located and constrained using satellite altimetry data (e.g. CMEMS, https://marine.copernicus.eu). Yet, satellite data are an orientation but often not satisfying to locate eddies for dedicated biogeochemical sampling (Fischer et al. 2021; Fischer et al. in preparation). To estimate the physical properties of the cyclonic eddy in our study, we used multi-section velocity data from a vessel-mounted Acoustic Doppler Current Profiler (vmADCP) data. Following previous studies (Casteleo and Johns 2011; Castelao et al. 2013; Bendinger et al. in preparation), we apply a nonlinear least-squares optimization to reconstruct the eddy within a cylindrical coordinate framework (Fig. **S1**). Briefly, assuming a radially axisymmetric, non-translating vortex the methodology optimizes the azimuthal velocity while coming up with an eddy center estimate. The estimated eddy center is then used to derive the radial azimuthal velocity structure before determining its radius and maximum azimuthal velocity. This characterization is based on the assumption of solid-body rotation, meaning that the azimuthal velocity linearly increases from the center toward the core-periphery (maximum swirl velocity, R1). Outside, toward the eddy periphery (R0), the velocity structure may be defined by a hyperbolic or exponential decay.

The radial structure of azimuthal velocity v_θ is given by

$$v_\theta = -u\sin(\theta) + v\cos(\theta),$$

where u and and v are the zonal and meridional velocities as measured by the vmADCP, and $\theta = \arctan((y - y_c)/(x - x_c))$ with (x, y) the position vectors of the velocity samples and (x_c, y_c) the eddy center coordinates. In the framework of solid-body rotation, the relative vorticity ζ_z is given by

$$\zeta_z = \frac{1}{r}\frac{\partial(r v_\theta)}{\partial r}$$

where r is the radius. The eddy periphery R0 is defined where $\zeta_z = 0$, i.e $\frac{\partial v_\theta}{\partial r} = -\frac{v_\theta}{r}$.

We determined the eddy center at [18.69 °N, 18.05 °W] with a core radius of 40.5 ± 5.7 km (Fig. S1) on the 22/07/19. However, the estimations of the eddy periphery from the three vmADCP sections showed high variability with a radius of the eddy periphery (R0) ranging

between 70 and 90km. Therefore we decided to define the stations inside the periphery of the eddy from the eddy-induced variability on surface temperature, salinity and chlorophyll a (Fig. **1b**,**c**,**d**).

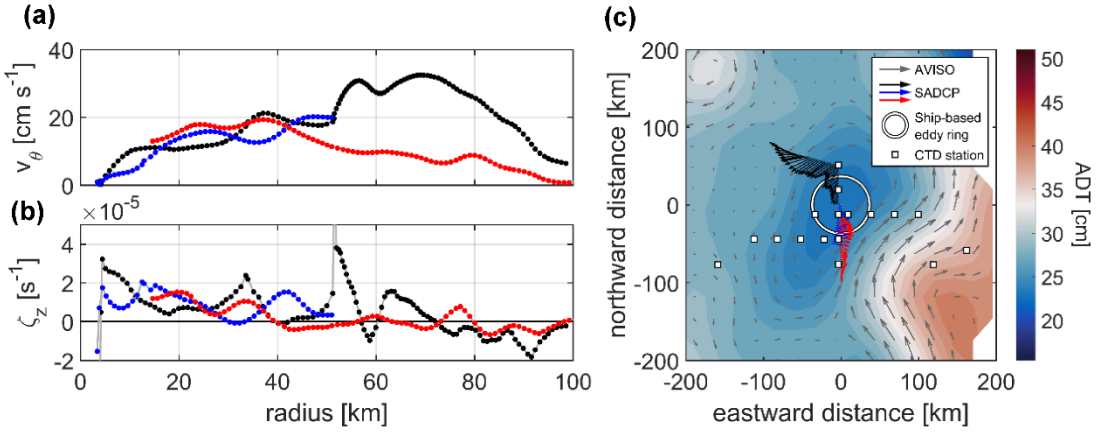

Figure S1: Mean 17.5-49.5 m radial profiles of (a) azimuthal velocity and (b) relative vorticity as a function of radius from the eddy centre as measured and derived by the 75 kHz vmADCP, (c) Background geostrophic velocity field (gray vectors) including absolute dynamics topography (ADT, shading) from 23 July 2019 downloaded from CMEMS. The eddy boundary (defined as the maximum azimuthal velocity) is given by the white circle where the coordinate origin represents the eddy center. Mean 17.5-49.5 velocity vectors for three ship transects across the eddy taking place from 21 July 2019 15:46:00 to 22 July 14:16:00 (black, blue) and from 25 July 2019 15:25 to 25 July 2019 19:47 (red), respectively. Undertaken CTD stations are marked by the white squares.

Taking into account the movement of the CE with an average speed of 3 km d^{-1} (Schütte et al. 2016), and the sampling date, the stations within the core-periphery were characterized as "core" and those outside the core and within the eddy-influenced area as "periphery" (SI table **1**). An anticyclonic eddy was forming along the Mauritanian Coast (core, 17.7°N, 17°W) and was interfering with the velocity field of the CE (Fischer et al. 2021; Fischer et al. in preparation). As the anticyclonic eddy was not fully detached from the coast we considered the stations within it to be still representative of the coast and we characterize them as "coastal" (SI Table **1**). Although not reliable for the exact localization of the cores and diameter of eddies, surface height anomaly showed that St. E3 was in the middle of two cyclonic eddies. Therefore St. E3 was likely to be influenced by the phenomenon of frontogenesis and was characterized as a "Frontal Zone". Stations located offshore not likely to be influenced by eddies were defined as "open ocean".

Table n°1: Characteristic of M156 sampling stations

Station	Date	Time (UTC)	Longitude (°W)	Latitude (°N)	Position	Mixed layer depth (m)	Distance from the eddy center (km)
E1	07/04/2019	07:58	-24,33	18,00	Open ocean	31	>200
S1	07/05/2019	05:00	-23,61	18,00	Open ocean	32	>200
S2	07/08/2019	04:58	-22,78	18,00	Open ocean	29	>200
E2	07/07/2019	03:48	-22,00	18,00	Open ocean	31	>200
S3	07/09/2019	05:51	-21,13	18,00	Open ocean	29	>200
S4	15/07/2019	04:00	-20,30	18,00	Open ocean	25	>200
E3	14/07/2019	04:00	-19,55	18,00	Frontal Zone	24	176
EDZ-1	17/07/2019	20:50	-19,11	18,29	Periphery	7	118
EDZ-2	17/07/2019	23:55	-18,83	18,29	Periphery	11	92
EDZ-3	19/07/2019	02:10	-18,54	18,29	Periphery	20	67
EDM-4	19/07/2019	07:30	-18,37	18,58	Core	23	34
EDZ-4	18/07/2019	19:50	-18,26	18,29	Periphery	21	50
EDM-2E	21/07/2019	19:00	-18,08	19,15	Periphery	23	48
EDM-5E	24/07/2019	06:35	-18,08	18,29	Periphery	22	47
EDM 3E	22/07/2019	00:42	-18,08	18,87	Core	26	16
S5	23/07/2019	22:18	-18,08	18,00	Periphery	12	79
EDM 4E	22/07/2019	09:15	-18,08	18,58	Core	22	15
EDZ-5N	26/07/2019	02:15	-17,97	18,58	Core	19	19
EDZ-6N	26/07/2019	08:55	-17,68	18,58	Periphery	15	44
EDZ-7N	26/07/2019	22:00	-17,39	18,58	Periphery	6	73
EDZ-8N	28/07/2019	06:26	-17,11	18,58	Periphery	14	103
S6	29/07/2019	01:17	-16,92	18,00	Coastal	20	145
EDZ-10N	27/07/2019	18:07	-16,53	18,58	Coastal	12	162
E5	27/07/2019	06:00	-16,52	18,17	Coastal	20	175

Table n°2: Abundance of eukaryotic picoplankton (Euk Pico G1), eukaryotic nanoplankton (Euk nano G2, Euk nano G3 and chrytophyta G5) and cyanobacteria *Prochlorococcus* (*prochlo*) and *Synechococcus* (*Synecho* G4) during M156. All abundances unit are 10^6 cell L^{-1}.

Station	Depth (m)	Lon (°W)	Lat (°N)	*Prochlo*	Euk pico G1	Euk nano G2	Euk nano G3	*Synecho* G4	Chrypto G5
E1	5	-24,33	18,00	0,27	0,80	1,09	0,02	3,87	0,04
E1	25	-24,33	18,00	2,07	2,72	1,17	0,01	3,92	0,05
E1	75	-24,33	18,00	65,93	73,96	4,58	0,08	0,15	0,03
E1	125	-24,33	18,00		0,93	0,08	0,01	0,04	0,03
E1	200	-24,33	18,00		0,07	0,01	0,00	0,01	0,02
S1	5	-23,61	18,00		1,24	1,05	0,03	4,97	0,06
S1	25	-23,61	18,00		3,77	1,10	0,03	4,98	0,06
S1	75	-23,61	18,00		49,01	3,16	0,05	0,05	0,05
S1	125	-23,61	18,00		1,96	0,18	0,01	0,01	0,01
S1	200	-23,61	18,00		0,06	0,00	0,00	0,01	0,01
S2	5	-22,78	18,00		6,64	2,23	0,08	132,75	1,13
S2	25	-22,78	18,00		46,28	3,20	0,10	113,64	0,98
S2	45	-22,78	18,00	220,26	236,32	10,61	0,21	25,26	0,62
S2	100	-22,78	18,00		4,00	0,28	0,01	0,19	0,05
S2	200	-22,78	18,00		0,15	0,01	0,00	0,10	0,01
E2	5	-22,00	18,00	10,30	8,19	4,25	0,10	59,70	0,40
E2	25	-22,00	18,00	7,40	8,13	4,21	0,07	59,24	0,36
E2	50	-22,00	18,00	64,61	94,52	10,44	0,13	44,20	0,40
E2	100	-22,00	18,00		0,89	0,21	0,00	0,57	0,04
E2	200	-22,00	18,00		0,12	0,05	0,00	0,15	0,07
S3	5	-21,13	18,00	7,87	13,91	7,62	0,10	121,85	0,37
S3	25	-21,13	18,00		44,97	9,19	0,12	93,14	0,30
S3	50	-21,13	18,00		44,48	7,53	0,31	3,03	0,20
S3	100	-21,13	18,00		2,22	0,28	0,00	0,75	0,04
S3	200	-21,13	18,00		0,16	0,05	0,00	0,34	0,05
S4	5	-20,30	18,00		14,70	7,14	0,09	314,54	1,11

Table n°2 cont.: Abundance of eukaryotic picoplankton (Euk Pico G1), eukaryotic nanoplankton (Euk nano G2, Euk nano G3 and chrytophyta G5) and cyanobacteria *Prochlorococcus* (*prochlo*) and *Synechococcus* (*Synecho* G4) during M156. All abundances unit are 10^6 cell L^{-1}.

Station	Depth (m)	Lon (°W)	Lat (°N)	*Prochlo*	Euk pico G1	Euk nano G2	Euk nano G3	*Synecho* G4	Chrypto G5
S4	25	-20,30	18,00		17,08	6,33	0,10	270,50	0,97
S4	35	-20,30	18,00		51,99	7,51	0,33	99,73	0,73
S4	100	-20,30	18,00		1,21	0,18	0,01	0,34	0,05
S4	200	-20,30	18,00		0,17	0,04	0,00	0,51	0,03
E3	5	-19,55	18,00	0,32	5,69	9,92	0,42	14,47	1,44
E3	25	-19,55	18,00	3,07	7,56	6,87	0,51	10,68	0,95
E3	45	-19,55	18,00	13,62	18,08	6,47	0,24	16,70	0,66
E3	90	-19,55	18,00		0,51	0,45	0,03	0,69	0,08
E3	200	-19,55	18,00		0,17	0,04	0,00	0,36	0,03
EDZ-1	5	-19,11	18,29	0,32	0,69	1,27	0,16	19,93	1,02
EDZ-1	27	-19,11	18,29	0,90	2,87	1,42	0,27	12,39	1,71
EDZ-1	50	-19,11	18,29	0,33	2,23	0,43	0,01	1,08	0,21
EDZ-1	100	-19,11	18,29		0,37	0,13	0,01	0,49	0,15
EDZ-1	200	-19,11	18,29		0,27	0,03	0,01	0,40	0,10
EDZ-2	5	-18,83	18,29		1,00	1,75	0,15	37,43	0,76
EDZ-2	15	-18,83	18,29		1,32	2,42	0,23	62,77	1,32
EDZ-2	50	-18,83	18,29		1,31	0,33	0,01	1,48	0,15
EDZ-2	100	-18,83	18,29		0,29	0,09	0,01	0,88	0,12
EDZ-2	200	-18,83	18,29		0,21	0,05	0,00	0,54	0,04
EDZ-3	5	-18,54	18,29		0,99	1,46	0,14	21,84	0,73
EDZ-3	25	-18,54	18,29		1,83	0,56	0,04	4,75	0,50
EDZ-3	33	-18,54	18,29		1,28	0,37	0,01	3,05	0,23
EDZ-3	60	-18,54	18,29		0,55	0,12	0,00	1,27	0,12
EDZ-3	150	-18,54	18,29		0,21	0,03	0,00	0,21	0,05
EDM-4	5	-18,37	18,58		19,60	6,08	0,75	360,78	5,88
EDM-4	23	-18,37	18,58		20,27	5,83	0,68	349,98	5,92
EDM-4	40	-18,37	18,58		3,38	1,59	0,05	11,19	0,50
EDM-4	100	-18,37	18,58		0,20	0,05	0,00	0,62	0,04

Table n°2 cont.: Abundance of eukaryotic picoplankton (Euk Pico G1), eukaryotic nanoplankton (Euk nano G2, Euk nano G3 and chrytophyta G5) and cyanobacteria *Prochlorococcus* (*prochlo*) and *Synechococcus* (*Synecho* G4) during M156. All abundances unit are 10^6 cell L^{-1}.

Station	Depth (m)	Lon (°W)	Lat (°N)	*Prochlo*	Euk pico G1	Euk nano G2	Euk nano G3	*Synecho* G4	Chrypto G5
EDM-4	200	-18,37	18,58		0,15	0,03	0,00	0,38	0,04
EDZ-4	5	-18,26	18,29		14,11	1,05	0,25	78,46	1,30
EDZ-4	26	-18,26	18,29		17,12	1,78	0,21	81,37	3,39
EDZ-4	35	-18,26	18,29		1,52	0,48	0,03	1,73	0,22
EDZ-4	100	-18,26	18,29		0,28	0,07	0,01	0,68	0,09
EDZ-4	175	-18,26	18,29		0,21	0,03	0,00	0,31	0,04
EDM-2E	5	-18,08	19,15		9,25	4,00	0,68	161,39	1,42
EDM-2E	30	-18,08	19,15		6,44	2,85	0,67	59,56	1,76
EDM-2E	45	-18,08	19,15		12,59	1,62	0,03	2,01	0,16
EDM-2E	100	-18,08	19,15		0,30	0,05	0,01	0,16	0,10
EDM-2E	200	-18,08	19,15		0,34	0,10	0,01	0,23	0,09
EDM-5E	5	-18,08	18,29		9,74	6,19	0,55	223,60	8,16
EDM-5E	20	-18,08	18,29		19,21	2,81	0,17	79,31	2,75
EDM-5E	32	-18,08	18,29		0,99	0,61	0,03	2,99	0,29
EDM-5E	40	-18,08	18,29		1,20	0,41	0,01	1,41	0,16
EDM-5E	100	-18,08	18,29		0,24	0,04	0,00	0,45	0,07
EDM-3E	5	-18,08	18,87		20,93	7,64	1,11	387,07	4,41
EDM-3E	20	-18,08	18,87		20,62	7,48	1,04	327,21	4,51
EDM-3E	38	-18,08	18,87		3,08	5,87	0,09	11,54	0,68
EDM-3E	50	-18,08	18,87		0,35	0,42	0,02	0,94	0,10
EDM-3E	150	-18,08	18,87		0,22	0,07	0,00	0,42	0,06
S5	5	-18,08	18,00		6,91	6,57	0,11	123,33	0,61
S5	25	-18,08	18,00		17,98	11,16	0,27	363,00	4,56
S5	32	-18,08	18,00		19,37	11,75	0,32	377,85	5,18
S5	50	-18,08	18,00		1,47	0,79	0,05	2,31	0,27
S5	200	-18,08	18,00		0,18	0,05	0,00	0,51	0,08
EDM-4E	5	-18,08	18,58		33,52	8,91	0,34	621,81	8,25
EDM-4E	15	-18,08	18,58		29,42	7,47	0,29	415,08	5,79

Table n°2 cont.: Abundance of eukaryotic picoplankton (Euk Pico G1), eukaryotic nanoplankton (Euk nano G2, Euk nano G3 and chrytophyta G5) and cyanobacteria *Prochlorococcus* (*prochlo*) and *Synechococcus* (*Synecho* G4) during M156. All abundances unit are 10^6 cell L^{-1}.

Station	Depth (m)	Lon (°W)	Lat (°N)	*Prochlo*	Euk pico G1	Euk nano G2	Euk nano G3	*Synecho* G4	Chrypto G5
EDM-4E	35	-18,08	18,58		2,43	2,35	0,03	4,49	0,27
EDM-4E	60	-18,08	18,58		0,32	0,19	0,01	0,86	0,08
EDM-4E	200	-18,08	18,58		0,17	0,05	0,00	0,31	0,06
EDZ-5N	5	-17,97	18,58		67,33	8,96	0,39	741,36	10,14
EDZ-5N	20	-17,97	18,58		45,39	5,78	0,40	458,39	8,94
EDZ-5N	30	-17,97	18,58		0,72	1,27	0,07	3,03	0,35
EDZ-5N	100	-17,97	18,58		0,19	0,05	0,01	0,66	0,05
EDZ-5N	200	-17,97	18,58		0,17	0,02	0,00	0,69	0,08
EDZ-6N	5	-17,68	18,58		11,86	4,35	0,35	267,15	4,57
EDZ-6N	14	-17,68	18,58		8,53	1,48	0,16	31,98	1,86
EDZ-6N	44	-17,68	18,58		0,51	0,84	0,01	2,28	0,18
EDZ-6N	100	-17,68	18,58		0,25	0,11	0,00	2,12	0,13
EDZ-6N	200	-17,68	18,58		0,17	0,07	0,00	0,81	0,05
EDZ-7N	5	-17,39	18,58		1,80	2,33	0,59	274,47	1,41
EDZ-7N	20	-17,39	18,58		7,50	1,88	0,45	273,86	1,59
EDZ-7N	40	-17,39	18,58		0,35	0,40	0,03	3,51	0,23
EDZ-7N	75	-17,39	18,58		0,28	0,10	0,00	3,56	0,15
EDZ-7N	170	-17,39	18,58		0,17	0,03	0,01	1,28	0,08
EDZ-8N	5	-17,11	18,58		2,95	6,58	0,39	642,99	2,80
EDZ-8N	17	-17,11	18,58		14,81	10,72	0,54	1079,84	6,01
EDZ-8N	40	-17,11	18,58		0,41	0,30	0,01	1,12	0,17
EDZ-8N	125	-17,11	18,58		0,31	0,12	0,00	1,90	0,12
S6	5	-16,92	18,00		9,32	4,91	0,19	13,11	0,31
S6	28	-16,92	18,00		40,19	17,29	0,20	24,59	0,39
S6	50	-16,92	18,00		17,20	13,21	0,13	72,63	1,06
S6	130	-16,92	18,00		1,95	0,53	0,01	1,60	0,09
EDZ-10N	10	-16,53	18,58		3,16	2,39	0,05	48,53	0,33
EDZ-10N	20	-16,53	18,58		3,63	2,31	0,03	57,46	0,29

Table n°2 cont.: Abundance of eukaryotic picoplankton (Euk Pico G1), eukaryotic nanoplankton (Euk nano G2, Euk nano G3 and chrytophyta G5) and cyanobacteria *Prochlorococcus* (*prochlo*) and *Synechococcus* (*Synecho* G4) during M156. All abundances unit are 10^6 cell L^{-1}.

Station	Depth (m)	Lon (°W)	Lat (°N)	*Prochlo*	Euk pico G1	Euk nano G2	Euk nano G3	*Synecho* G4	Chrypto G5
EDZ-10N	44	-16,53	18,58		78,20	13,03	0,18	102,19	2,15
EDZ-10N	75	-16,53	18,58		7,10	1,45	0,02	3,16	0,16
EDZ-10N	119	-16,53	18,58		0,59	0,20	0,01	2,24	0,19
E5	5	-16,52	18,17	4,37	5,97	1,56	0,05	63,10	0,46

Community respiration using the optode-based method

The most used technique to determine the trophic state of a system (autotrophy or heterotrophy) is the Winkler method with dark-light bottle incubation from which gross primary production and community respiration rates ratio is obtained (GPP/CR; e.g. Regaudie-de-Gioux et al. 2012). But the Winkler method is time-consuming and to study BR, a filtration step is mandatory which causes two major problems, oxygen contamination of the samples and an overestimation of BR by removing the protistan grazer (Aranguren-Gassis et al. 2012). Shorter incubation with *in-vivo* ETS method (Martínez-García et al. 2009) reducing filtration impacts had shown that Community respiration (CR) and BR are tightly correlated even in the oligotrophic area (Aranguren-Gassis et al. 2012). However, such techniques still distort water oxygen properties and therefore are not suitable when it comes to investigating oxygen minimum zones, which occurred in our case. Optode-method was therefore a suitable option in terms of precision, rapidity of implementation, and ability to maintain water properties.

Optodes were glued to the inside surfaces of Winkler-bottles using silicone cement (Warkentin et al. 2007). We allowed the silicone to cure for 2 days at room temperature. Before the cruise, we performed a two-point calibration of optodes according to the manufacturer's instructions using air-saturated and temperature-equilibrated samples and oxygen-depleted samples obtained by dissolving Na_2SO_3 into Milli-Q water (10g L^{-1}). We measured the photoluminescence lifetime of the luminophores within sensor spots by a fiber-optic oxygen meter (Fibox 3; PreSens GmbH) fixed outside of the bottle opposite to inside sensor spots. We supplied excitation light (505 nm), which also transported the emitted fluorescence signal (600 nm) back to the oxygen meter (Warkentin, 2007). We incubated optodes bottles at 14°C in the dark for at least 24h and with at least four-time point measurements. We followed the

temperature inside bottles with a Pt100 Temperature Sensor (Presens) to monitor temperature acclimation. Oxygen concentrations were measured every 2s during an interval of 3 to 5 minutes and data were recorded using OxyView 7.01 (PreSens GmbH). Bottles were rinsed between each set of incubations with 4-5% HCL (manufacturer indication) and five times with 18 MΩ Mili-Q. Incubations were initiated by transferring seawater to the glass bottles using standard gas sampling techniques to avoid oxygen contamination. Site-specific values for salinity compensation of the oxygen readings were obtained from cabled CTD casts. Oxygen measurements were corrected using the Presens oxygen calculator with the mean temperature value measured at each time point (in extra temperature-control bottles) and with the *in-situ* salinity to determine the absolute [O_2] values. [O_2] values precision was validated by comparison of values measured directly after sampling and CTD oxygen data corrected with Winkler titrations (Fig. S**2**) for the same depth.

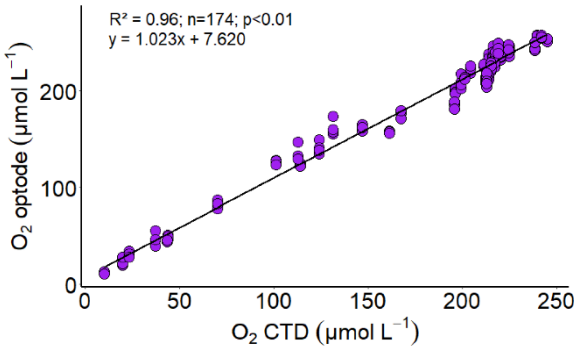

Figure S2: Linear correlation between calibrated oxygen values obtained from the CTD and oxygen concentration measured with optode directly after sampling during the community respiration experiments.

We determined the drift commonly occurring with optode-based methods (Wikner et al. 2013; Vikström et al. 2019) by collecting and filtering seawater through 0.2µm nucleopore filters which were incubated in the dark like the samples. Non-linear oxygen dynamics are frequent in oxygen measurement, (Briand et al. 2004, Vikström et al. 2019) in both natural and manipulated samples. Therefore, Akaike information criteria (AIC; Snipes and Taylor 2014) was used to determine when nonlinear oxygen dynamics occurred. Then a quadratic polynomial (Eq. 1) was fitted to the data:

$$[O_2] = C + at + bt^2 \quad \text{(Eq. 1)}$$

Here, $[O_2]$ is the absolute oxygen concentration at time t, C the y-axis intercept, and *a* and *b* are coefficients. As oxygen respiration is assumed to be linear, daily CR was calculated using the difference of the linear (or quadratic polynomial) regression between t0 (after temperature acclimation) and 24 h. We obtained a detection limit of CR of 0.62 µmol O_2 L^{-1} d^{-1} by taking the standard error of the oxygen decline (SE_{sample}) and residual standard error in 0.2 µm filtered seawater ($SE_{background}$) into account and using SE_{Total} as a detection limit according to Eq.2:

$$SE_{Total} = \sqrt{SE_{samples}^2 + SE_{background}^2} \text{ (Eq.2)}$$

Extrapolation of ex-situ BP and CR rates at 22°C

As we measured the microbial activities at different incubation temperatures for technical concern, we decided to convert the values of BP and CR at 22°C because we could not successfully extrapolate the PP_{TOT} rates to in-situ temperature. For that we used equations from López-Urrutia and Morán for BP (BP_U; 2007; Eq.5) and from Regaudie de Gioux and Duarte for CR (CR_{RG}; 2012; Eq.7).

$$BP_U = \left[e^{-0.589/(kT)} \times \left[\frac{2.33 \times 10^{11} chl\ a}{chl\ a + 4.08} + 6.77 \times 10^9\right]\right] \times Bacterial\ abundance \text{ (Eq. 5)}$$

Temperature and resource availability effects on cell-specific bacterial metabolism, with k, the Boltzmann's constant (8.617734 10^{-5} eV K^{-1}), T the water temperature (°K), chl *a*, the *in-situ* chlorophyll *a* concentration in µg L^{-1} and *in-situ* bacterial abundance in cell L^{-1}.

$$Ln^{\left(\frac{CR_{RG}}{chl\ a}\right)} = -0{,}66 \times \left(\frac{1}{kT}\right) + 27{,}72 \text{ (Eq.6)}$$

$$CR_{RG} = e^{Ln^{\left(\frac{CR}{chl\ a}\right)}} \times chl\ a \text{ (Eq.7)}$$

The linear relationship between the natural logarithm of the volumetric specific chlorophyll a-CR rates ($\frac{CR}{chla}$ in mmol O_2 mg Chl a^{-1} d^{-1}) within 1°C bin and the inverted water temperature (1/kT with k, the Boltzmann's constant (8.617734 10^{-5} eV K^{-1}) and with T, the water temperature (°K)). CR_{RG} (µmol O_2 L^{-1} d^{-1}) was then obtained from the exponential of the natural logarithm of the volumetric specific chlorophyll a-CR rates multiplied by the *in-situ* chlorophyll *a* (Chl *a* in µg L^{-1}).

Then, we compared the rates of BP and CR measured *ex-situ* ($BP_{ex-situ}$ and $CR_{ex-situ}$) with the rates obtained from BP_U and CR_{RG} calculated at the temperature set during the incubations (Fig. **S3**). It was 14°C for BP and for CR (~14°C) they are listed in table **3**. The rates obtained from the equations (BP_U and CR_{RG}) were significantly correlated (Fig. **S3**) and within the ranges of the rates measured with *ex-situ* incubations ($BP_{ex\text{-}situ}$ and $CR_{ex\text{-}situ}$). Therefore, we used the correlation between BP_U and CR_{RG} rates (Fig. **S4**) calculated at the incubation temperature and at 22°C to extrapolate BP and CR at 22°C:

$$BP_{22°C} = BP_{14°C} \times 0{,}996$$

$$CR_{22°C} = CR_{14°C} \times 2.011 - 0.013$$

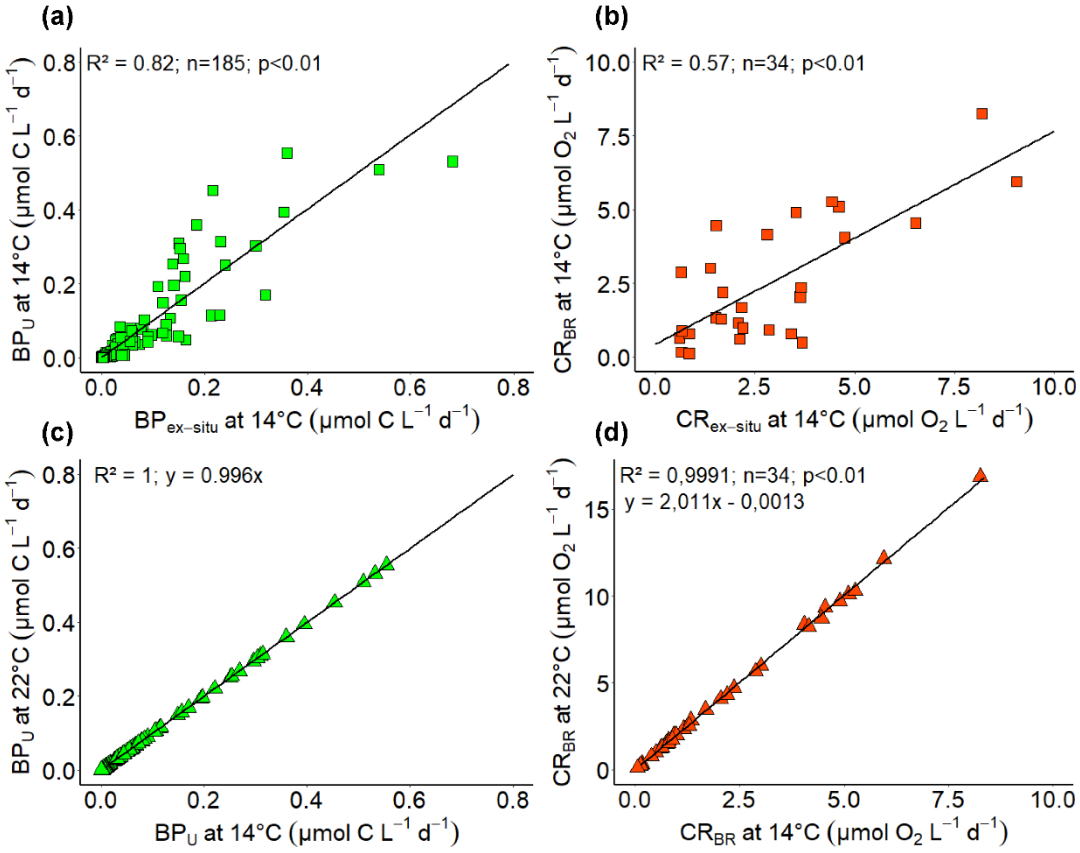

Figure S3: Linear relationship between BP_U and CR_{RG} rates calculated at the temperature measured during *ex-situ* incubation (14°C for BP, see table **S2** for CR) and the ex-situ BP (**a**) and CR rates (**b**) and linear relationship between BP_U and CR_{RG} rates calculated at the temperature measured during *ex-situ* incubation (14°C for BP, see table **S2** for CR) and 22°C, (**c**) and (**d**).

174 Table n°3: Average and standard deviation (SD) of temperature measured during community
175 respiration experiments.

Station	Depth (m)	Incubation temperature		Station	Depth (m)	Incubation temperature	
		Average	SD			Average	SD
E1	5	13,91	0,12	EDM-4	5	14,43	0,01
	25	13,86	0,14		23	14,43	0,03
	75	13,90	0,13		40	14,40	0,03
	125	13,86	0,17		100	14,42	0,04
E2	5	14,13	0,10	EDM-4E	5	14,55	0,02
	25	14,15	0,09		15	14,56	0,02
	50	14,17	0,12		35	14,56	0,02
	100	14,15	0,12		60	14,55	0,01
S3	5	13,55	0,15	EDZ-5N	5	14,43	0,12
	25	13,56	0,16		20	14,41	0,12
	50	13,59	0,19		32	14,42	0,11
	100	13,53	0,15		100	14,39	0,13
E3	5	14,01	0,05	EDZ-7N	5	14,33	0,06
	25	13,96	0,06		25	14,35	0,06
	45	13,98	0,06	E5	5	14,49	0,05
	90	14,02	0,06		15	14,49	0,04
EDZ-2	5	14,10	0,05		35	14,49	0,05
	15	14,10	0,05				
	50	14,09	0,05				
	100	14,10	0,05				

176

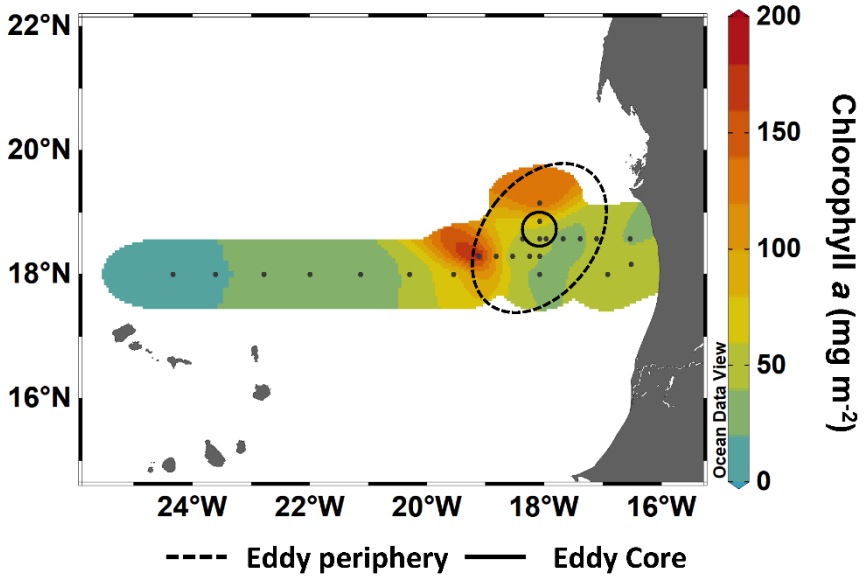

177

178 Figure S4: Integrated Chlorophyll *a* over 100m depth.

179

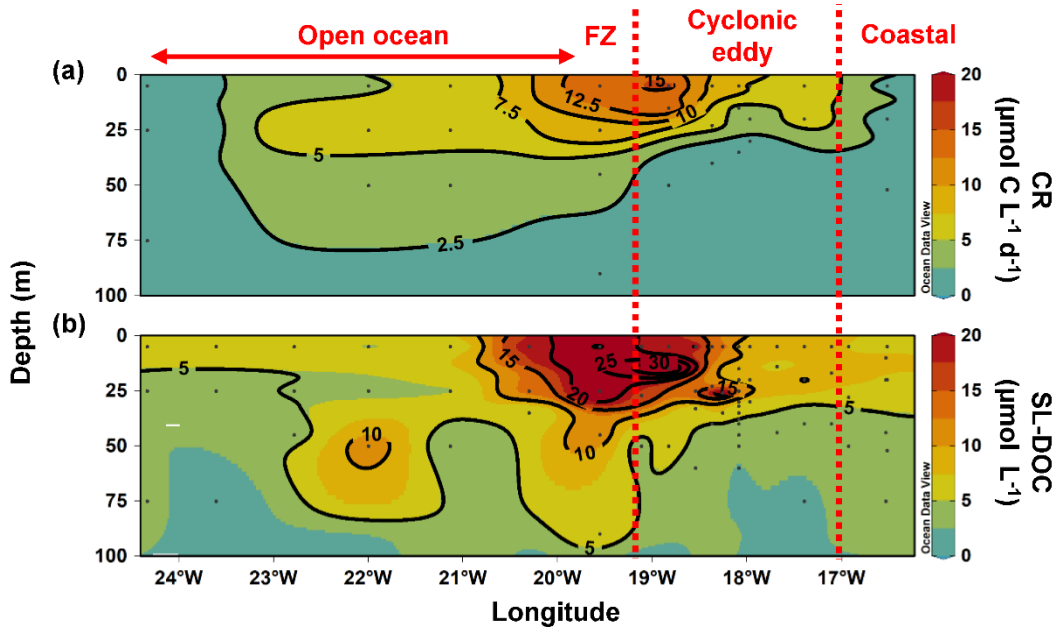

180

181 Figure S5: depth distribution of (**a**) community respiration and (**b**) Semi-labile dissolve organic carbon
182 (SLDOC) over 100m depth. Red dashed line show the eddy-influenced area and FZ refer as Frontal
183 Zone.

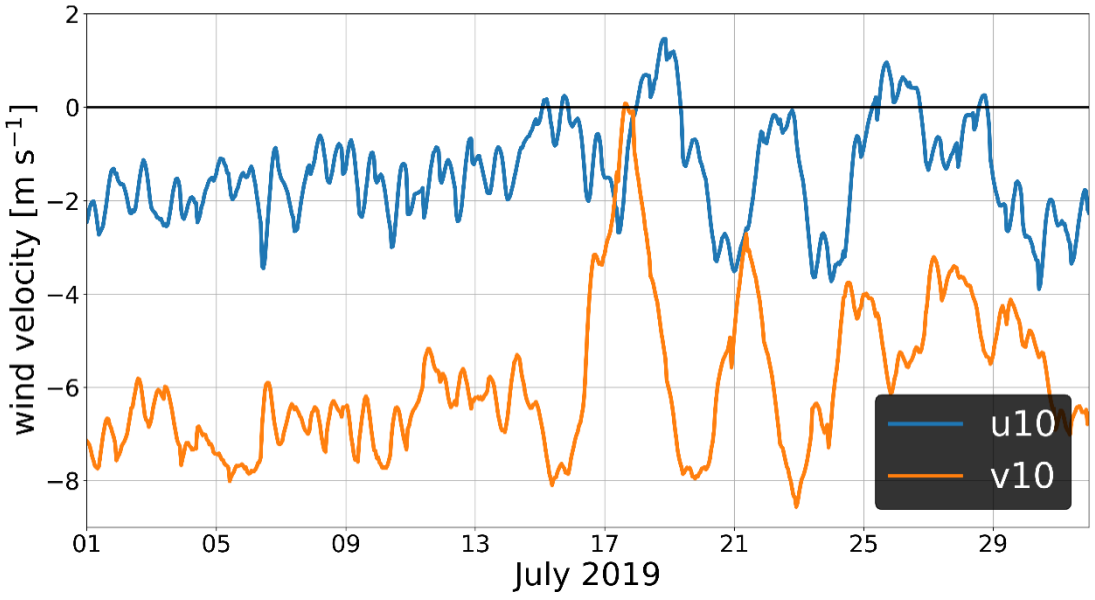

Figure S6: Domain averaged (25W-16W, 16N-22N) eastward (u10) and northward (v10) component of the 10m wind. Data were obtained from ERA5 database (Hersbach et al., 2018)

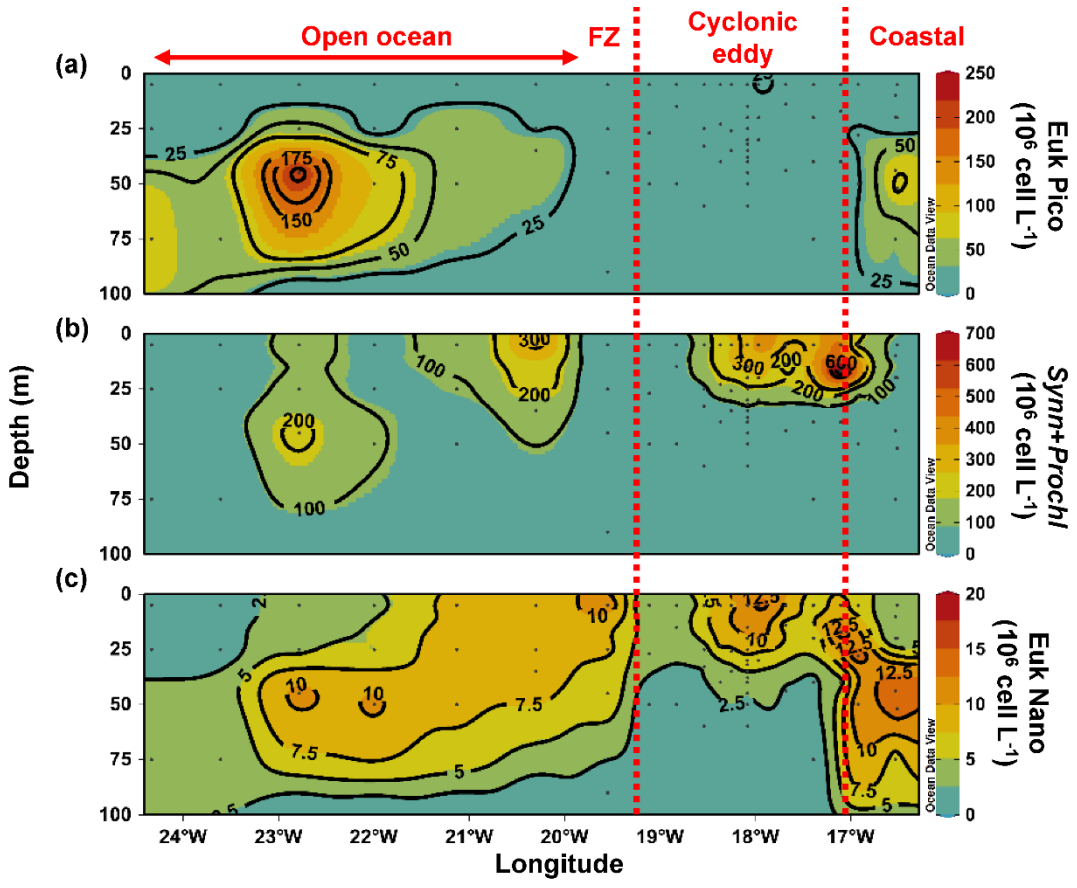

Figure S7: depth distribution of (**a**) eukaryotic picoplankton abundance, (**b**) sum of cyanobacteria *prochlorococcus* and *synechococcus* abundance, (**c**) sum of eukaryotic nanoplankton abundance (G2 and G3 and chryptophyta) over 100m depth. Red dashed line show the eddy-influenced area and FZ refer as Frontal Zone. see SI Table **2** for details.

193 Reference
194

195 Aranguren-Gassis, M., Teira, E., Serret, P., Martínez-García, S., and Fernández, E.: Potential
196 overestimation of bacterial respiration rates in oligotrophic plankton communities, Mar. Ecol.
197 Prog. Ser., 453, 1–10, https://doi.org/10.3354/meps09707, 2012.

198 Briand, E., Pringault, O., Jacquet, S., and Torréton, J. P.: The use of oxygen microprobes to
199 measure bacterial respiration for determining bacterioplankton growth efficiency. Limnol.
200 Oceanogr. Methods, 2(12), 406–416, https://doi.org/10.4319/lom.2004.2.406, 2004.

201 Fischer, T., Karstensen, J., Dengler, M., and Bendinger, A.: Multiplatform observation of
202 cyclonic eddies during the REEBUS experiment, EGU General Assembly 2021, online, 19–30
203 Apr 2021, EGU21-6537, https://doi.org/10.5194/egusphere-egu21-6537, 2021.

204 Hersbach, H., Bell, B., Berrisford, P., Biavati, G., Horányi, A., Muñoz Sabater, J., Nicolas, J.,
205 Peubey, C., Radu, R., Rozum, I., Schepers, D., Simmons, A., Soci, C., Dee, D., Thépaut, J-N.:
206 ERA5 hourly data on single levels from 1979 to present. Copernicus Climate Change Service
207 (C3S) Climate Data Store (CDS). (Accessed on 08-Oct-2021), 10.24381/cds.adbb2d47, 2018.

208 López-Urrutia, Á., and Morán, X. A. G.: Resource limitation of bacterial production distorts
209 the temperature dependence of oceanic carbon cycling, Ecology, 88(4), 817–822.
210 https://doi.org/10.1890/06-1641, 2007.

211 Martínez-García, S., Fernández, E., Aranguren-Gassis, M., and Teira, E.: In vivo electron
212 transport system activity: A method to estimate respiration in natural marine microbial
213 planktonic communities, Limnol. Oceanogr. Methods, 7, 459–469,
214 https://doi.org/10.4319/lom.2009.7.459, 2009.

215 Regaudie-De-Gioux, A., and Duarte, C. M.: Temperature dependence of planktonic metabolism
216 in the ocean, Glob. Biogeochem. Cycles., 26(1), 1–10. https://doi.org/10.1029/2010GB003907,
217 2012.

218 Snipes, M., and Taylor, D. C.: Model selection and Akaike Information Criteria: An example
219 from wine ratings and prices, Wine Econ. Policy, 3(1), 3–9.
220 https://doi.org/10.1016/j.wep.2014.03.001, 2014.

221 Vikström, K., Tengberg, A., & Wikner, J.: Improved accuracy of optode-based oxygen
222 consumption measurements by removal of system drift and nonlinear derivation, Limnol.
223 Oceanogr. Methods, 17(3), 179–189, https://doi.org/10.1002/lom3.10297, 2019.

Warkentin, M., Freese, H. M., Karsten, U., and Schumann, R.: New and fast method to quantify respiration rates of bacterial and plankton communities in freshwater ecosystems by using optical oxygen sensor spots, Appl. Environ. Microbiol, 73(21), 6722–6729, https://doi.org/10.1128/AEM.00405-07, 2007.

Wikner, J., Panigrahi, S., Nydahl, A., Lundberg, E., Båmstedt, U., and Tengberg, A.: Precise continuous measurements of pelagic respiration in coastal waters with Oxygen Optodes. Limnol. Oceanogr. Methods, 11, 1–15, https://doi.org/10.4319/lom.2013.11.1, 2013.